Manufacturing, assembly, and testing of scaled, historic masonry for one-gravity, pseudo-static, soil-structure experiments

Debra F. Laefer[1], James H. Long[2], Edward J. Cording[3], Aykut Erkal[4], and Linh Truong Hong[5]

[1]Tenured Lecturer and Lead Principal Investigator, Urban Modelling Group (UMG), School of Architecture, Landscape, and Civil Engineering (SALCE), University College Dublin (UCD), Dublin 4, Ireland; Phone: 353-1-716-3226; Fax: 353-1-716-3297; e-mail: debra.laefer@ucd.ie. Corresponding author.
[2]Associate Professor, Department of Civil and Environmental Engineering (CEE), University of Illinois at Urbana-Champaign (UIUC), Urbana, IL 61801, USA; Phone: 1-217-333-2543; Fax: 1-217-333-9464; e-mail: jhlong@illinois.edu
[3]Professor Emeritus, Department CEE, UIUC, Urbana, IL 61801, USA; Phone: 1-217-333-6938; e-mail: ecording@illinois.edu
[4]Post-doctoral Researcher, Department of Civil Engineering, University of Bath, UK; Phone: 353-1-716-3232; e-mail: ae301@bath.ac.uk
[5]Doctoral Candidate, UMG, SALCE, UCD, Dublin 4, Ireland; Phone: 353-1-716-3232; e-mail: linh.truong-hong@ucdconnect.ie

ABSTRACT: In many model-scale experiments, geometric scaling is upheld but kinematic and/or dynamic similitude is not because of the difficulty in manufacturing and assembling small models. This paper describes scaling, manufacturing, assembly, and testing of $1/10^{th}$ scaled historic masonry materials for one-gravity, pseudo-static, soil-structure testing. Prototype selection, manufacturing limitations, constructability constraints, and testing decisions are presented, alongside details related to model construction. Compressive, tensile, and shear capacities of one-tenth scale prototype values, as well as failure mechanisms, were achieved by adopting traditional brick extrusion and firing methods, in conjunction with modifying mortar products developed for historic restoration. When scaled-masonry structures were subjected to adjacent excavation, damage levels and patterns and levels were consistent with full-scale, field observations.

KEY WORDS: historic brick masonry, mortar, manufacturing, soil-structure, scaling, sand, adjacent excavation, cracks, preservation, conservation

1. Introduction

Small-scale testing is attractive, because it is faster and less expensive than large-scale or full-scale experiments. However, for reduced-scale experiments to be reliable, a model must respond like its prototype. To achieve this, geometric, kinematic, and dynamic relationships must be upheld. While geometric similarity is evident, kinematic and dynamic similarity are not always so. In dynamic testing, similarity requires all model velocity vectors and forces to have the same direction as the full-scale, with corresponding magnitudes related by a single scale factor [1, 2]. While in 1-gravity (1g), pseudo-static testing of masonry, the main problem is obtaining materials whose strength and stiffness are both sufficiently reduced compared to of those of the prototype. This is true for the individual elements and their composite behaviour, when assembled. There are also the usual constraints of constructability and material availability, which often

present competing factors and pose major challenges. Furthermore, when modelling historic masonry, the situation is additionally complicated by (1) the high variability of the original materials; (2) decades (if not centuries) of in-situ degradation; and (3) poor documentation of the performance characteristics of the original materials. This paper introduces new solutions for manufacturing, assembling, and testing historic scaled-masonry for 1g, pseudo-static, soil-structure experiments, the complexity of which does not easily lend itself to centrifuge work.

2. Prior solutions

In prior 1g, masonry testing, many researchers have ignored scaling requirements, because of difficulties in manufacturing small-scale units and constructing assemblages of reduced-strength material, thus potentially introducing unintended scale-effects [3]. Often this has been justified by relatively large (half-scale) testing or by reporting only qualitative outputs (e.g. crack patterns), but in some cases, no acknowledgment of the problem is made. A sampling of approaches is shown in Table 1.

Table 1. Properties of models used in experimental 1g masonry studies.

Area of Study	Scale	Model					Reference
		Geometry (mm)		f'_c (MPa)			
		Masonry unit L x H x W	Mortar Thickness	Unit	Mortar	Masonry	
Shear strength	1/3	97 x 63 x 47	3	30.31	9.06	10.20	Neto et al., 2008 [4]
Blast resistance	1/4	100 x 50 x 50	>2.5	14	12.4	NA	Dennis et al., 2002 [5]
Seismic loading	2/3	390 x 190 x 140	10-12	18.1	11.3	17.9	Laursen & Ingham, 2004 [6]
Seismic loading	1/5	78 x 58 x 38	~3	1.09	0.45	1.27	Tomazevic and Klemenc, 1997 [7]
Cyclic loading	1/3	95 x 95 x 65	7	7	3.8	6.6	Altin et al., 2008 [8]
Cyclic loading	1/3	93 x 60 x 60	~7.5	3.1	1.53	2.63	Kakaletsis and Karayannis, 2008 [9]
		95 x 52 x 45		26.4	1.75	15.18	
Seismic loading	1/10	29 x 18.5 x 13.5	~1	Not modelled			Turer et al., 2007 [10]
Cyclic loading	1/9	40 x 30 x 21	1	NA	NA	0.93	Manos et al., 1993 [11]
Retrofit	1/2	150 x 95 x 75	5	14.8	3.2	4.8	El Gawady et al. 2007 [12]
Seismic loading	1/4	65 x 30 x 30	2	6.06	0.46	2	Zarnic et al., 2001 [13]
Seismic resistance	1/5	78 x 58 x 38	~3	1.09	0.45	1.27	Tomazevic and Klemenc, 1997 [14]
Static loading	1/2	102 x 305 x 305	9.5	0.10	0.02	0.03	Henderson et al., 2003 [15]
Shear testing	1/6	50.8 x 25.4 x 15.9	3.2	30.4	8.1	NA	Murthy and Hendry, 1965 [16]
Physical properties	1/3	131 x 67 x 47	3.3	NA	NA	20.7	Harris et al., 1990 [17]
Seismic loading	3/8	94 x 45 x 28	5	46.4	NA	13.5	Abrams, 1997 [18]

NA: not available

3. Scaling requirements

To minimize (and eliminate, where possible) scale-effects when conducting model-scale work, the concept of dimensional homogeneity or similitude was pioneered by Buckingham [19] and extended by Rayleigh [20]. To accommodate the same behaviour in both prototype structure (p) and scaled model (m), material selections are predicated upon the similarity concept, for which scale factors were computed.

$$S_i = \frac{\text{i quantity in a scaled model}}{\text{i quantity prototype structure}} \tag{1}$$

In the proposed solution, the scaled model strains must be identical to the prototype model ones, for which the scale factor for strains that were computed based on the applied load and Young's modulus can be expressed as

$$\left(\frac{\sigma}{E}\right)_p = \left(\frac{\sigma}{E}\right)_m \tag{2}$$

In which σ and E are respectively normal stress and Young's modulus of materials, and p and m subscripts are represented to prototype and scale model.

In soil-structure model, applied soil surface stress must be reduced to ensure a stable soil mass beneath the structures. Soil overloading is a particular concern in the uppermost portion of the soil profile where confining stress is minimal because of the relatively small scale of the work, as previously described [21,22]. If the nature of the soil cannot be effectively change the stress in the building model must be reduce. For the building model to respond at the reduced stress akin to how the prototype responds under full-scale loading, the building materials' strength and stiffness must be. Herein, the scale factor for stress was adopted equal to a geometry scale ($S_\sigma = 1/n$). Therefore, equation (2) was re-written for building and soil materials as equation (3) and (4) respectively:

$$\left(\frac{1}{E_b}\right)_p = \frac{1}{n}\left(\frac{1}{E_b}\right)_m \tag{3}$$

$$\left(\frac{1}{E_s}\right)_p = \frac{1}{n}\left(\frac{1}{E_s}\right)_m \tag{4}$$

where b and s subscripts represent to quantity of the building and soil, 1/n is a scale factor of geometry of physical model.

Since loads on the model are transferred to the soil, stresses applied to the soil are the same as those on the model building's foundations (Eq. 5)

$$\sigma_{ss} = \sigma_b \tag{5}$$

where σ_{ss} is the applied stress on the soil surface, and σ_b is the stress applied through the building components at the soil-structure interface. This must address the fundamental understanding the sand gains strength and stiffness with depth (Eq. 6)

In non-cohesive soils, bearing capacity and deformability are assumed to be linear with depth (Eq. 6 and 7), as first proposed by Terzaghi [23], where q_a is net allowable load, q_d, is the design load, SF is the safety fact, γ is the soil unit weight, D_f is the foundation depth factor, B is the foundation width factor, and $N\gamma$ and N_q are the dimensionless bearing-capacity factors depending primarily on the soil's friction angle. Stress, σ_s, at a pint is proportional to the soil's elastic modulus E_s, unit weight γ, and depth H. Based on equations 6 and 7, the soil characteristics are considered to be linearly increasing with depth

$$q_a = \frac{q_d}{SF} = [\frac{\gamma N_\gamma}{2} + \gamma(N_q - 1)\frac{D_f}{B}]\frac{B}{SF} \tag{6}$$

$$\sigma_s \propto E_s \propto \gamma H \tag{7}$$

Thus, to meet the challenges of matching soil characteristics, model building materials must be manufactured with ultimate load capacities and stiffnesses of only 1/n of those of the full-scale prototype. Development of such materials is described in sections 4 and 5.

4. Experimental aims and prototype selection

To illustrate material selection and development, a portion of a larger testing program [22,24] to consider building response to adjacent excavation is herein described. A common urban scenario was selected, including a load-bearing, unreinforced masonry (URM) building with a semi-continuous, shallow foundation (Figs. 1 and 2).

Construction details were taken from historical records, including turn-of-the-century building manuals and guidelines showing 297.5 mm wide walls on foundations 2.5 times wider [25, 26,27,28] and assuming medium-hard bricks in lime mortar. Details of footing configuration and loading selection are reported elsewhere [29].

Masonry capacity is derived from individual components and their interaction. Consequently direct correlations between individual material properties and final composite performance is not assured. Thus, target values were selected initially for individual materials, as well as the composite masonry, with the strategy being that the individual materials would be tested first and once they were close to their target values they would be assembled and tested together. This process is not straight-forward, because behaviour between one set of engineering properties for historic masonry has not correlated well with others (e.g. shear and tension). Consequently, prototype selection was considered to be representative of a class of materials, namely early twentieth century American masonry, as opposed to matching of a specific building (Table 2).

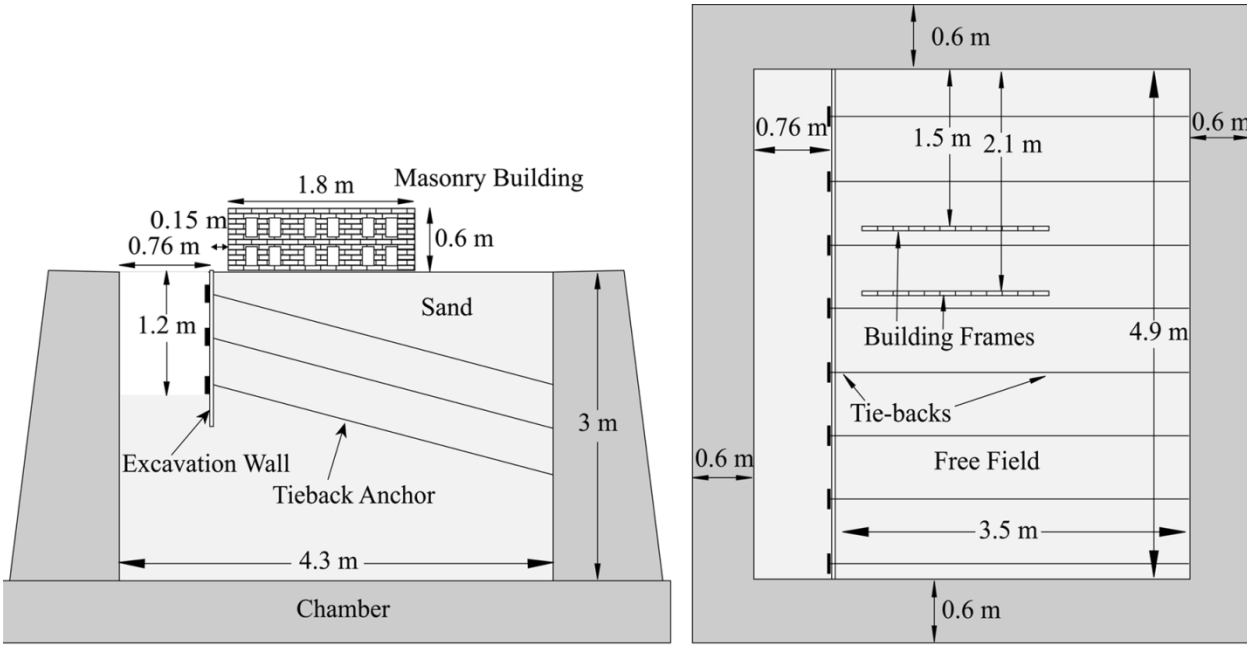

a) Section with continuous sheet-piling wall, masonry model building and anchors shown

b) Plan with continuous sheet-piling wall, masonry model building and anchors shown

Figure 1: a) Section; b) Plan of experimental set up [21]

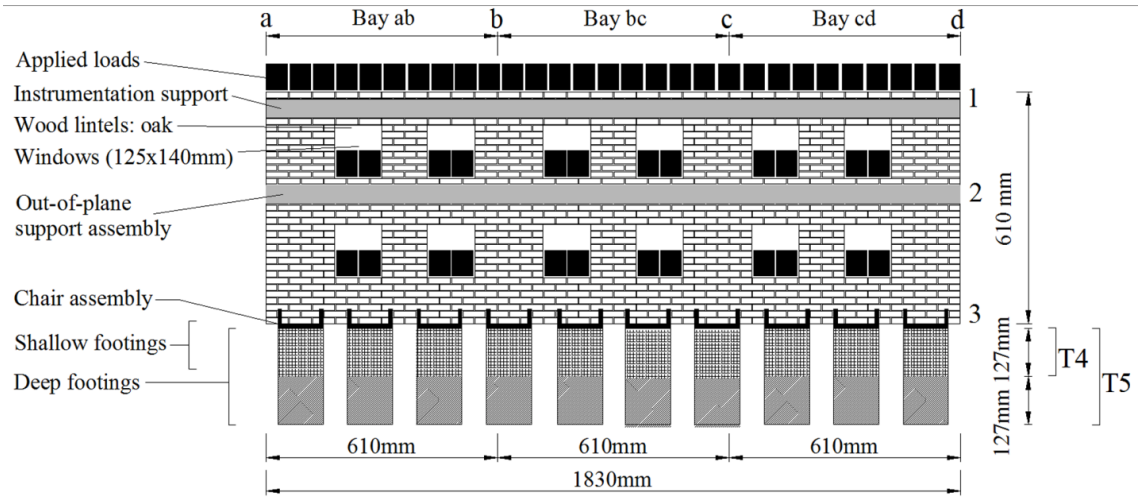

Fig. 2. Schematic details shown of masonry wall [21]

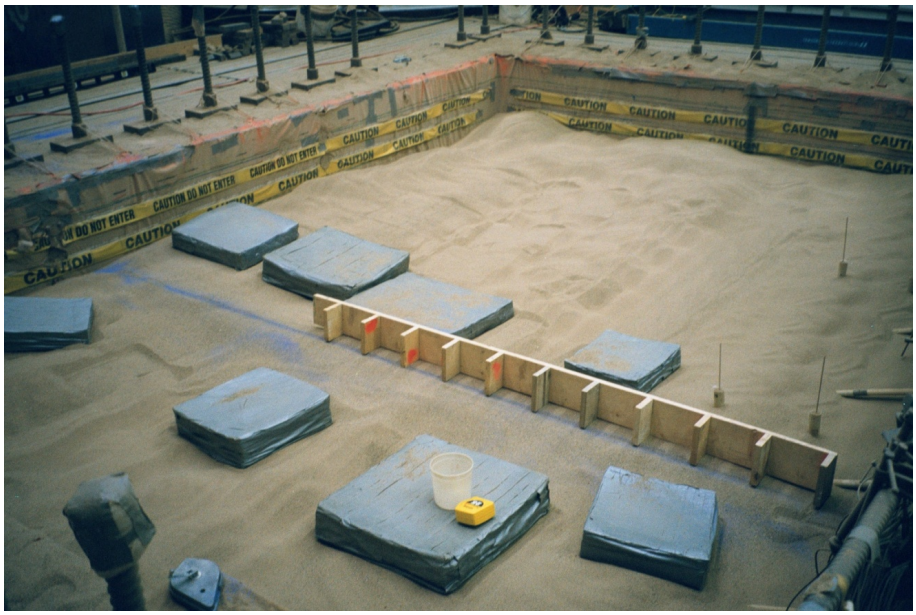

Fig. 3. Formwork shown for laying discrete URM footings.

Table 2. Expected prototype performance and resultant experimental values.

Property	Prototype	Target	Actual (average)
Brick compressive strength (tested longwise, no end preparation)	41.37-55.16 MPa	4.14-5.52 MPa	4.43 MPa*
Brick compressive strength (tested flatwise, no end preparation)	Not modelled due to lack of correlation between testing orientations	Not modelled	8.40 MPa
Brick modulus of rupture	8.62 MPa	0.86 MPa	0.39 MPa
Brick Poisson's ratio	.30	.30	.25
Brick absorption	No modelling needed	Not modelled	16.3%
Brick mass density	No modelling needed	Not modelled	1783.9 Kg/m^3
Brick Young's modulus	No prototype data available	Not modelled	81.28 MPa
Brick tensile strength	No prototype data available	Not modelled	5.00 MPa
Mortar compressive strength	6.89 MPa	0.69 MPa	1.31 MPa
Mortar tensile strength	1.37 MPa	0.13 MPa	0.15 MPa
Mortar Young's modulus	6894.76 MPa	689.48 MPa	5326.36 MPa
Mortar Poisson's ratio	No prototype data available	Not modelled	.30
Mortar mass density	Not modelled	Not modelled	1,557.9 Kg/m^3
Masonry compressive strength for 5 brick high prisms	22.34-23.99 MPa	2.23-1.71 MPa	4.14 MPa
Masonry Young's modulus	7763.50-10342.14 MPa	772.21-1034.21 MPa	1482.37 MPa
Masonry shear strength	0.38-0.53 MPa	0.04-0.05 MPa	0.05 MPa
Masonry flexural bond	0.59-0.82 MPa	0.06-0.08 MPa	Untestable

*Measured at first crack

5. Model material selection, manufacturing and assembling

5.1 Sand

The scale of the testing system required 40 tons of sand for its operation, and no scalable material for the soil was found that could be handled and placed reliably in such quantities. As such the selected sand was taken from a river deposit quarry near Pekin, Illinois. The sand was washed and kiln dried at the quarry. According to the Unified Soil Classification system, the model sand was a poorly graded sand (SP) with coefficient of uniformity (C_u) of 2.64 and a coefficient of curvature (C_c) of 1.12 [22]. The CPT test was carried out on three samples and tip resistances were ranged 2.76MPa to 4.14MPa, in which the tip resistances showed generally linear increase of resistance with depth. Laboratory samples produced dense, medium, and loose mass densities corresponding to 1826kg/m^3 (a void ratio of 0.48), 1618kg/m^3 (a void ratio of 0.67) and 1586kg/m^3 (a void ratio of 0.71), respectively, with friction angles varying 32° to 55° for applied stresses of 6.9kPa to 68.9kPa by using direct shear tests.

5.2 Excavation wall

The excavation wall was 1.52m deep by 4.0m wide constructed of three pieces of 2.4 mm thick sheet metal. The pieces were attached by a continuous wale consisted of a 2.5cm x 2.5cm square tube at each tie back level. The excavation wall was set 0.76m from the front of the testing chamber (Figure 1). The excavation wall was supported by three levels of anchors equidistantly in vertical and horizontal directions (Figure 1). Vertical levels of the anchors were set uniform distance of 0.305m and the first level was appeared at 0.178m and 0.305m corresponding to 1.22m and 1.09m of the deep excavation for Test 4 and 5 (as will be described later), respectively. The ground surface in Test 5 was 0.13m lower than that in Test 4 with no change in the anchor layout [22]. The anchors were installed 15° from horizontal and made of 76.2mm diameter stainless steel rod. The unbonded portion of each was encased in a PVC tube.

5.3. Masonry Building Materials

Extensive testing was conducted to develop mortar and brick to meet performance- and constructability-related demands.

5.3.1 Mortar

Beyond strength and stiffness requirements, mortar was subjected to consistency and curing constraints. Consistency had to be adequately viscous to be a bedding material, while fluid enough for regular placement. Curing had to be sufficiently slow to allow many bricks to be laid with each batch of mortar but fast enough to lay multiple brick lifts each day. Additionally, only minimal, shrinkage-based cracking was allowed, to ensure continuous load transfer and to prevent problems identifying the displacement-based cracking anticipated during testing.

A preslaked, lime putty-based, restoration mortar by GenLime was selected as the binder/base material. Its 25% water content (by weight) required special additives and curing to prevent excessive shrinkage-induced cracking. Shrinkage in full-scale masonry is usually controlled by aggregate quantity and type. However, even a small amount of sand substantially interfered with workability. Workability issues also precluded lowering strength with an over-sanding approach – having insufficient binder for the aggregate to fully bind (Fig. 4). Several fillers were tried including flour, baking soda, baking powder, crushed limestone dust, silt, and glass microspheres. None produced a workable mortar that could be consistently placed with a uniform mortar joint thickness. Instead, small amounts of bentonite and air entrainment were added to the mix but no aggregate. Table 3 shows the final mix; mortar is usually described as parts per volume but weight was selected in this case, to ensure repeatability. The strength of the selected mix is shown in the context of other mixes using various levels of air entrainment and bentonite.

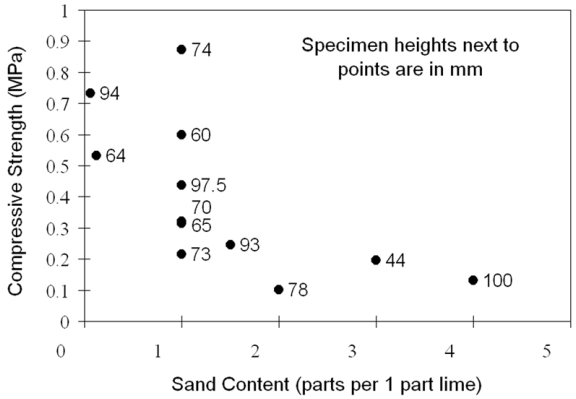

Fig. 4. Oversanding in lime mixes.

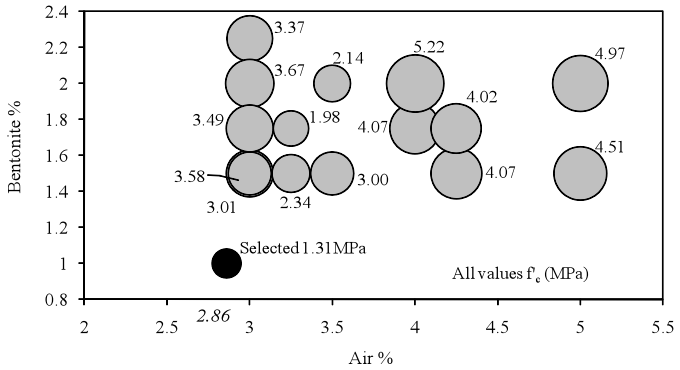

Fig. 5. Mortar strength as a function of bentonite and air entrainment levels.

Table 3. Mortar mix by weight and parts.

Component	Weight (g)	Percentage (%)
Bentonite	87.5	1.0
Air Entrainment	250.0	2.9
Lime Putty	5000.0	57.1

The bentonite absorbed some water prior to curing, which minimized shrinkage and increased stiffness, thereby allowing daily, multi-lift construction. The air entrainment (gumtree resin sold under the trade name DeVaar by W.R. Grace) served as a plasticizer and retarder, substantially delaying curing and causing significantly fewer cracks – either due to protracted curing or because the air entrainment encouraged more evenly distributed shrinkage. In many markets this product, under the same name, contains a resin from a tree other than the gum tree. When that product was used, no beneficial impact occurred.

Where possible ASTM standards C109/C109M [28] and C270 [29] were followed, but the fundamental differences in lime putty from dry lime and cement-based mortars precluded com-

plete compliance and resulted in three points of divergence in the mortar testing. The first difference was mixing time. Lime putty mortars showed no visible difference after 5-minute mixings versus the prescribed 35-minutes, so only 5 minutes were used. The second was that the putty's high water content with no off-setting aggregate resulted in too much shrinkage to cast testable samples using standard 50.8 mm x 50.8 mm cube moulds (Fig. 6). Thus, cubes were cut with a band saw from oversized samples cast in plastic buckets (Fig. 7). This permitted intact sample extraction from larger and partially cracked specimens. Cutting did not induce micro-cracking, as mortar cubes consistently broke in a catastrophic manner. Because of reduced air exposure for the mortar within the larger sample, cubes were tested at 35 days, instead of 28. A 35-day strength proved identical as the same as year-old samples. The third sample preparation difference was that 30 seconds of vibration was substituted for the rodding requirement because of the lime's propensity to adhere to the chumming rod.

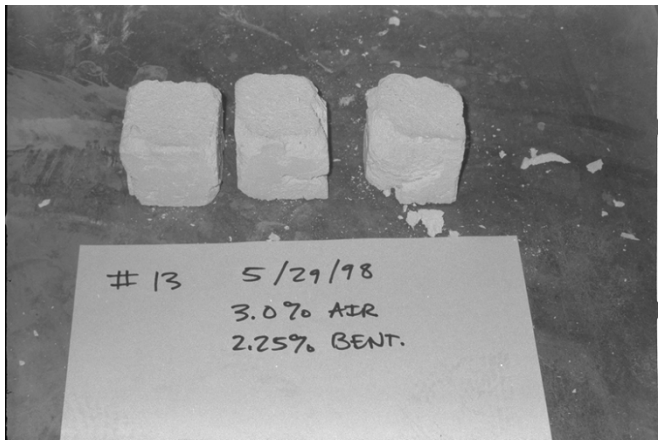

Fig. 6. Mortar cubes resulting from casting in 5.1cm x 5.1cm brass moulds.

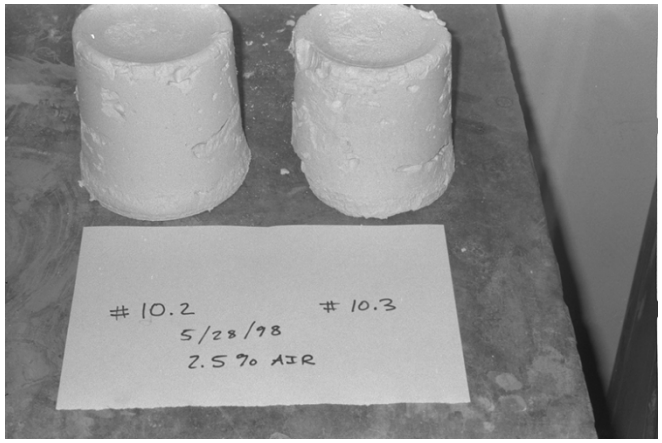

Fig. 7. Oversized cast mortar samples from which 5.1cm x 5.1cm samples were cut.

The exposed surface area of the mortar greatly impacted its full curing time, as carbonation, instead of hydration (as with cementious mixtures), was the curing method. For the model-sized

joints, 35 days was set as a minimum curing time based on laboratory tests and previous work [32].

Average compressive strength was 1.31 MPa, approximately twice the 0.69 MPa target strength. This mix had the lowest strength of any of those found to meet the constructability issues. Thus, the testing program proceeded with this mix as the closest available match. To further reduce the masonry strength, a slightly wider joint width was selected (as will be described in section 5.4).

All production mortar was made during two mixing sessions by the same researcher to increase consistency. Putty was always scooped from the bottom of each 22.68 kg pail and drained of any standing free water. The mortar could be stored indefinitely in re-sealable plastic bags even with the additives, because of the lime's carbonation based curing process. The wet, stored mortar showed no signs of change, even after one year, as long as the bag remained sealed and without holes.

5.3.2. Brick

Ribar and Dubovoy's [33] study of nearly 500 specimens (10 brick types and 20 mortar mixes) concluded that brick surface was the controlling factor for bonding characteristics, with brick microstructure (e.g. surface roughness, porosity) predominating. Thus, model brick production followed traditional manufacturing and construction processes, whenever possible. Unit extrusion and stationary kiln firing were considered essential aspects. The smallest commercially available extruded unit available was $1/4^{th}$ scale (57.15mm long x 28.58mm wide x 15.88mm high) - as opposed to the $1/10^{th}$ scale selected for the laboratory work. These quarter-scale extruded units were wrapped in plastic to prevent premature drying and shipped raw by Belden Brick Co. of Canton, Ohio to the University of Illinois at Urbana-Champaign's Ceramics Engineering Department, where they were fired.

Prior to firing, the bricks were dried for at least 24 hours at 65.6° C. They were fired in a stationary kiln with electrical heating elements on 5 sides (Fig. 8), based upon Belden Brick's proprietary firing schedule. Within each kiln, bricks were placed in 2 masses, each 463.55mm x 596.90mm x 127.00mm high (approximately 1,400 bricks per firing). Firing occurred at 496.1°C (verified via Orton cone #09) for at least 12 hours, with an additional day of kiln time for cooling. Firing heat and duration were minimized to limit strength gain, while providing sufficient sinter to prevent the units from returning to clay when exposed to water. Restricting strength augmentation was particularly challenging given that the flat-wise, compressive strength of a dried but unfired brick regularly reached 1.22 MPa, and the target scaled strength was only 4.14-5.52 MPa.

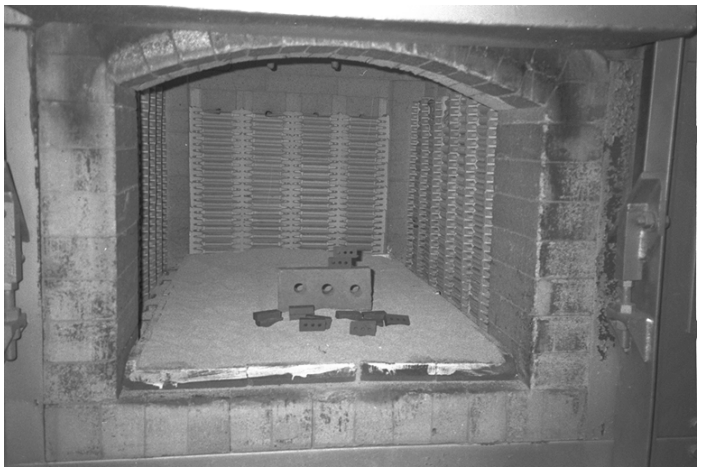

Fig. 8. Quarter-scale bricks shown in comparison to prototype brick in stationary, electric kiln.

Bricks were culled after firing to minimize the impact of brick variability on the model walls' structural performance. As part of this, each brick was individually inspected for defects (cracks, chips, or deformations), sorted by colour using a six gradation set of distinctions, and included only if dimensionally and visually acceptable. The kiln's oxidizing (as opposed to reducing) atmosphere facilitated a direct correlation between colour and strength. Colour designations were referred to in the experimental work as 0 to 5, but more precisely defined using a Munsell colour chart (Table 4). Those that exhibited two distinct bands of colour (due to kiln stack position) were described with two numbers (e.g. 3/4). The designations were as follows: 0 for a dried but unfired unit; 1 under-fired; 2 or 3 (depending on colour) for the least fired bricks that did not significantly lose strength and consistency when exposed to water, and exhibited relatively low strength variability (Fig. 9). Approximately half the bricks ranged between 2 and 3 (Fig. 10); they were both used in the model and were subsequently referred to as 2-3 bricks, as they spanned the colour range of those that were 2 and/or 3. Units beyond 3 were excluded, as they exhibited a higher strength, higher incidences of laminations, and barely visible, pre-test cracking. Under-fired units could be re-fired, although yield of usable units was lower than from the initial firing. End-wise tested bricks averaged a compressive strength of 4.43 MPa in the 2-3 group based on the proportion of bricks used in the 2 and 3 categories of bricks. Crushing or ultimate strength was substantially higher, up to three times depending upon orientation, but was not a concern, as the intention was to generate cracking through the mortar joints, as would have been consistent with the intent of historical construction practices.

Table 4. Munsell colour chart description of bricks.

Laboratory Designation	**0**	**1**	**2**	**3**	**4**	**5**
Munsell Hue Page	5 yellow grey	7.5 yellow red	5 yellow red	5 yellow red	2.5 yellow red	2.5 yellow red
Munsell Classification	8/2	7/4	6/8	6/8	6/8	5/10

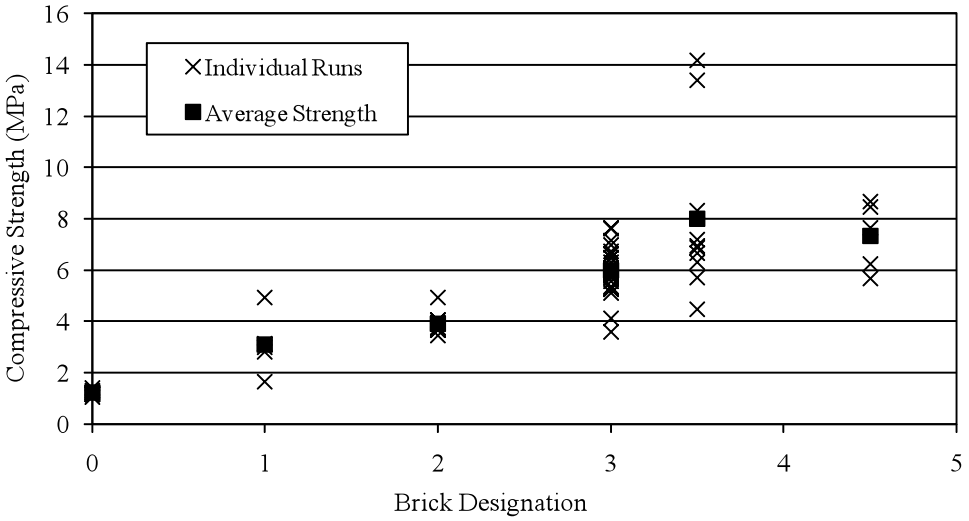

Fig. 9. Brick compressive strength by colour designation.

Initially, the individual bricks were capped prior to compressive testing in accordance with ASTM C67 [34]. When compared to specimens tested with sanded ends and those without any end preparation, those without end preparation were indistinguishable from the capped ones, with the added benefit of replicating historical data collection methods (Fig. 11). Finally, a full brick was tested instead of a half brick, because of the small unit size; traditionally half bricks were favoured because of testing machine load limits.

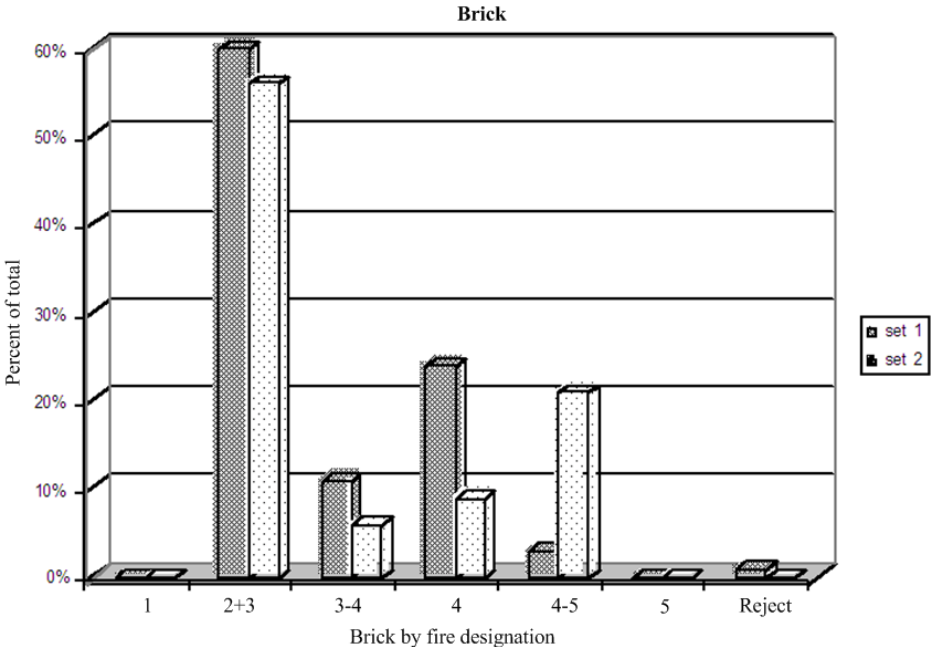

Fig. 10. Kiln yield by colour designation.

The Modulus of rupture (f_r') value was established in accordance with ASTM C67. The average was 144.8 kPa (flat-tested) and 627.4 kPa (edge-tested). Tensile capacity determined by testing units end-wise with a no-moment connection averaged 1.26 MPa for the 2-3 bricks (connector detail and broken bricks shown if Fig. 12). Absorption was 16.31%, but this value and much of those in the early literature may be better categorized as saturation potential and should not to be confused with initial rate of absorption, which requires a boiling portion to the test, which could not be performed because of disintegration problems because of the bricks' low sintering levels. Bricks were strain gauged to obtain the material's tangent Young's modulus (81.28 MPa) and Poisson's ratio (0.25).

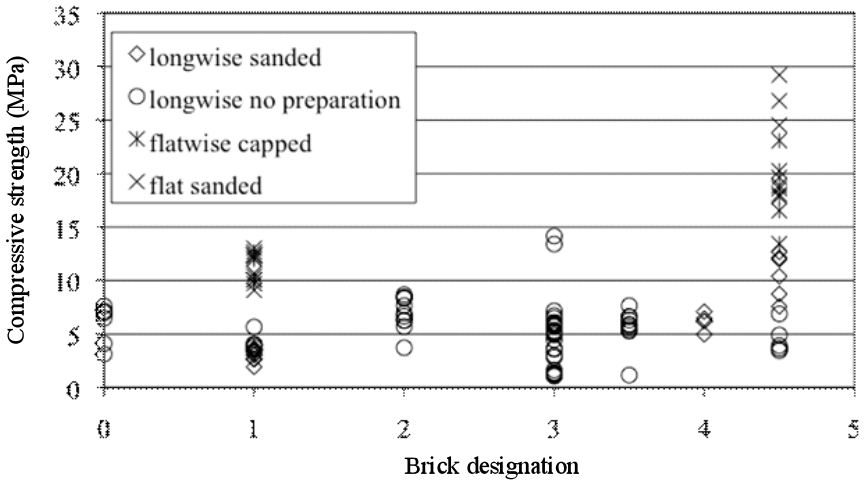

Fig. 11. Comparative compressive strength by end condition.

Fig. 12. Photograph of tensile brick testing.

5.5. Masonry

In accordance with standard industry practice, five-unit high prism tests were tested in compression giving an average compressive strength for the assemblage. Peak strengths ranged from 4.14 MPa to 6.89 MPa for 14 to 30 days with some strength loss and increased scatter at around 28 days; because of the joint thinness (as opposed to the comparatively large mortar cubes) a 28-day strength was targeted but problems with the testing equipment resulted in testing on day 30, instead. The strength variation observed was consistent with data by Rao [35] on lime mortar prisms, where high-lime content samples exhibited strength decreases after 28 days and observations by Pieper and Trautsch [36] of slight decreases in shear strength after at 28 days. Long-term studies on the selected mortar samples showed no significant changes between 35 and 365 days.

Masonry shear capacity depends on unit shape, size, absorption level, and bond mechanism. Work by Ritchie and Davison [37] showed how shear capacity may be equal for disparate conditions (e.g. a unit uniformly covered in low-strength mortar and a unit patchily covered with a higher strength mortar) and that determining the controlling factor is extremely difficult because of the interdependent nature of the variables. Average model-scale shear stress for laboratory triplets tested with no normal force was 46.2 kPa (Fig. 13), a strong match to the 482.6 kPa prototype value.

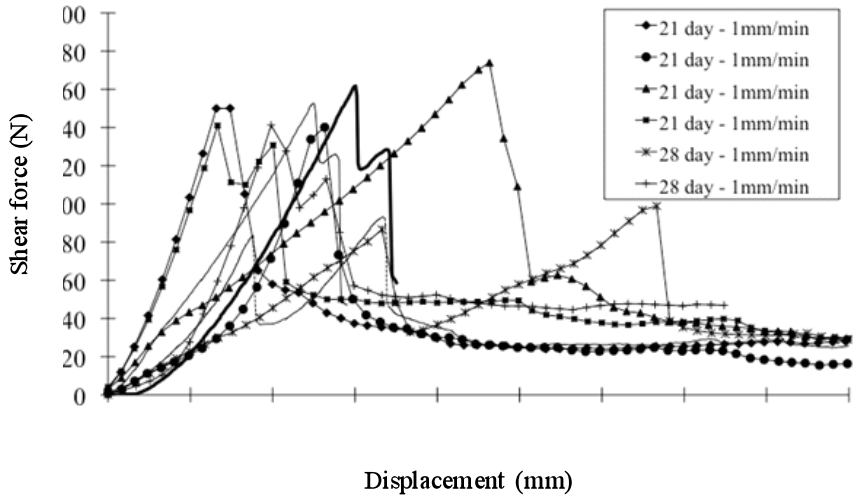

Fig. 13. Shear testing results on triplets with no confining stress at 21 and 28 days

In the absence of a viable tensile testing standard for low-strength masonry, pre-production and post-production test samples were made as couplets and pulled with a no-moment connection (Fig. 14); the samples would not have withstood coring through the centre of one brick and vertical joint directly above, as is often recommended. Scatter was large – ranging from less than 13.8 kPa to nearly 137.9 kPa with typical results being 48.3 kPa to 55.2 kPa.

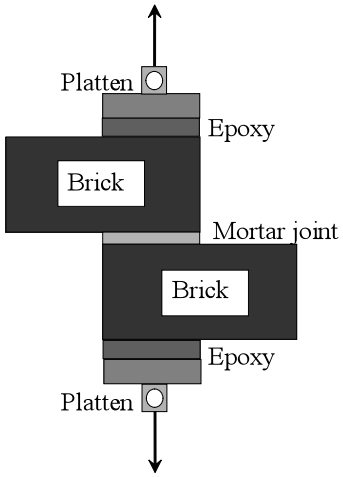

Fig. 14. Tensile testing via a no-moment connection.

5.5. Geometric Divergences

Due to the extruded brick size, the model units dimensionally scaled closer to a concrete block than a brick, thereby resulting in single-wythe construction. From a practical standpoint this resulted in a well-constructed wall, where damage patterns could be easily tracked and documented, and it avoided three-dimensional (3D) complications in an otherwise plane-strain testing program, as is the typical configuration for adjacent excavation testing arrangements. The 28.58 mm width of the single model brick was equivalent in width to a thickness of 2.5 wythes at $1/10^{th}$ scale. Many older structures were not assembled originally with as much care and diligence as might be either assumed or hoped. Consequently, the model walls performed in a somewhat idealized behaviour of all wythes working together. Since the mortar generally controlled both the cracking pattern and propagation, the behaviour of the single-wythe wall was not fundamentally different from a well-built prototype. This was confirmed during testing, where breakage occurred only in the mortar joints (Fig. 15). The testing was a progressive excavation as described in section 6.

A second area of dimensional divergence was the model's joint width. Head joint and bed joint thicknesses were 3.21 mm and 2.25 mm, respectively. This was scaled to the quarter-scale brick unit size. Selected joint thicknesses fell within the higher scaled-range of typical construction [38, 39] and permitted two important things: easier damage detection and assurance that the damage would predominate in the mortar; work by Lenczner [40] demonstrated that increased joint width decreased masonry strength for joint widths less than 16mm (for full-scale work). The larger experimental joint width resulted in an overall lowering of ultimate masonry capacity, which more closely emulated the masonry's target strength and stiffness.

Fig. 15. Close up of damaged URM wall at end of testing; cracks coloured post-test with marker after being measured.

Instrumentation of five-course high, brick prisms yielded an average modulus of elasticity of 107.94 MPa (Fig. 16), a value extremely close to 1/10th of the prototype (Table 2). The specimens proved too fragile to be subjected to ASTM E518 [41] for flexural bond strength testing. So no further attempts were made to quantify this.

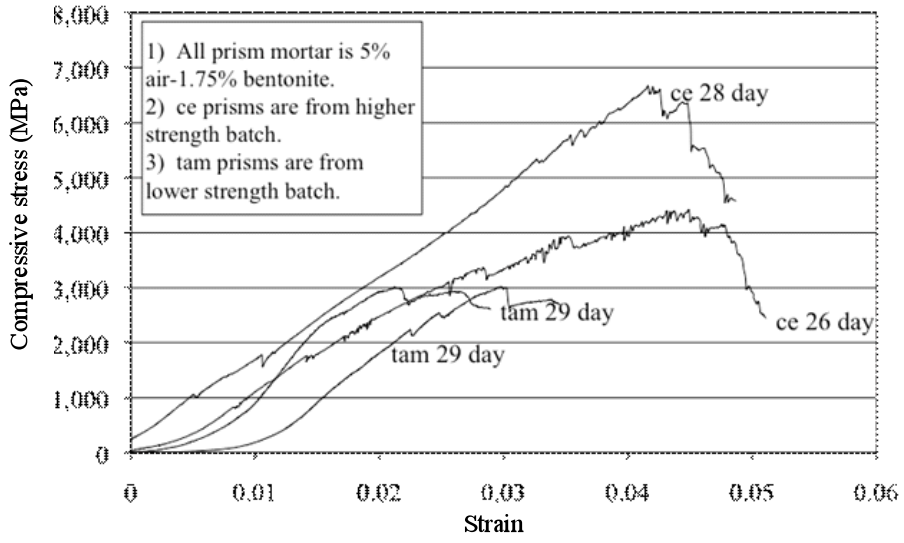

Fig. 16. Examples of Young's modulus of five-course high brick prisms.

5.6. Wall Construction

The brick walls (610 mm high, 1830 mm long, and 29.75 mm wide) were built in a large, frame inclined approximately 20° from vertical, to counter the walls' tendency to cure towards the air and curl, especially along the most freshly laid rows. Prior to initiating assembly, a laminated, computer-aided design (CAD) generated template of the wall was secured to the dismountable frame (Fig. 17). The template was an exact, scaled representation of the wall layout and provided a constant means to visually check unit placement and joint thickness at all points. Upon wall construction, no deviations from the template were visible. Prior to bricklaying, the template was covered by a thin sheet of wax paper to prevent sticking between the laminate and the brick. This was removed after the model was positioned in the testing chamber (Fig. 18 and 19).

Bricklaying was done as traditionally as possible, to replicate prototype construction. As such, all bricks were submerged in water for at least 4 minutes (maximum of 30), before being laid. The time was established experimentally and verified visually; the bricks stopped bubbling, when saturation was complete. After 30 minutes, brick disintegration began, because of low firing levels. Thus 30 minutes represented the maximum allowable soaking time for the brick. Failure to pre-wet the bricks sufficiently generated extreme mortar dehydration and prevented placement of an adequately, thin mortar layer; lime putty in a non-desiccatory environment can still be workable after several hours.

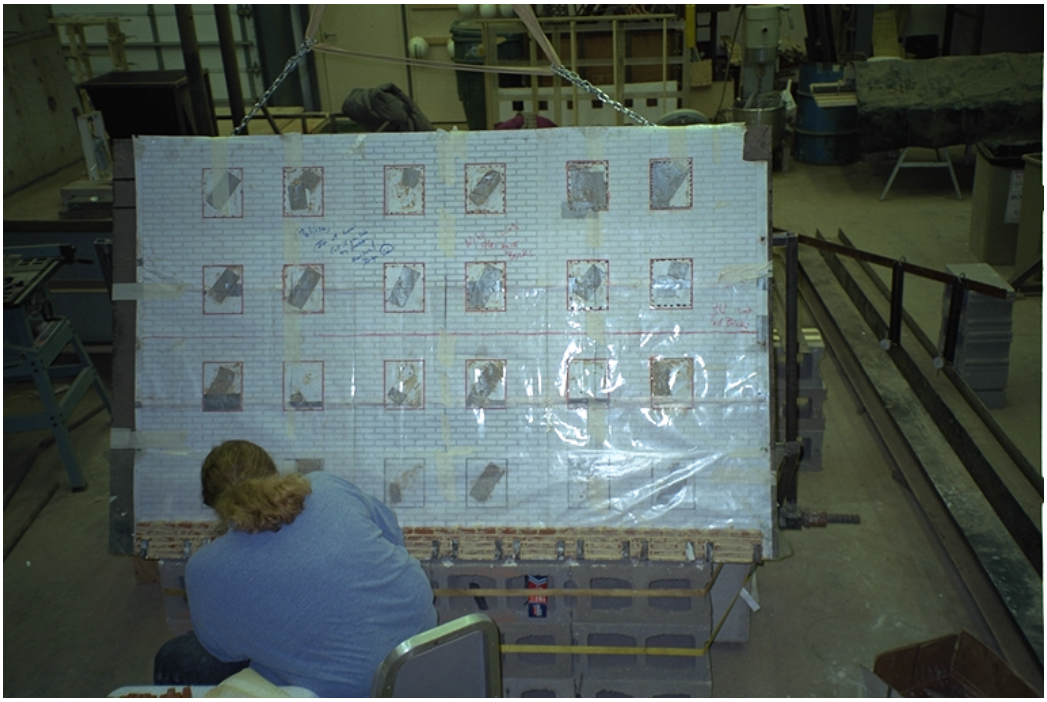

Fig. 17. Photograph of bricks being laid (formwork set for up to 4 storeys).

Fig. 18. Two model walls shown in their transport frames.

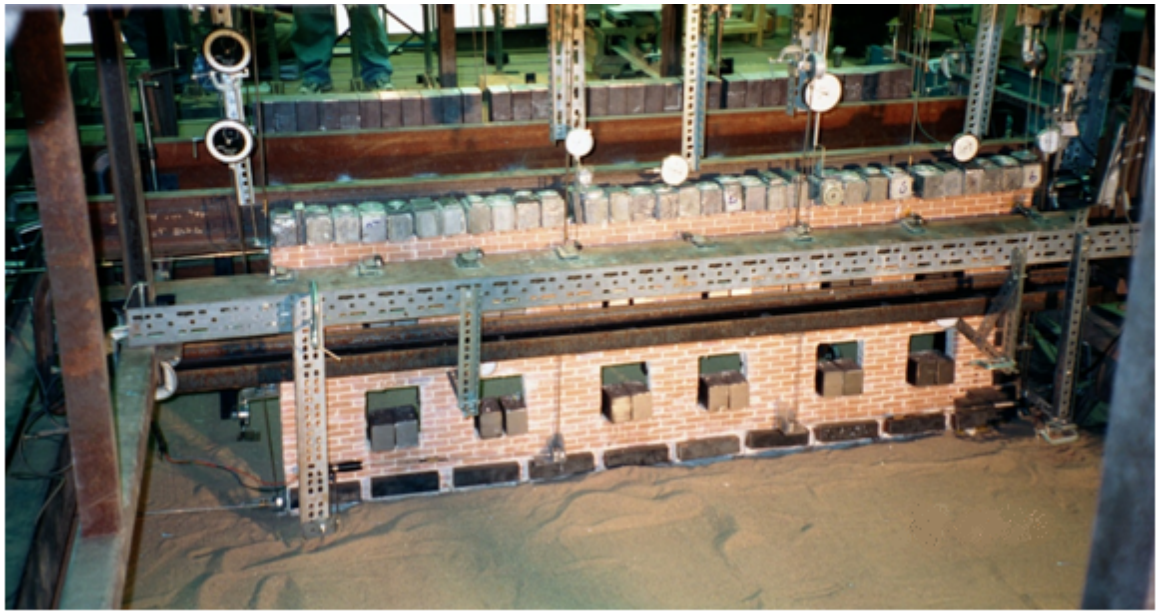

Fig. 19. Wall in place awaiting testing.

To ensure full bonding, each brick head was "buttered" with a small knife. This brick was then "shoved" up against the prior brick; thereby emulating full-scale bricklaying techniques. After being properly positioned left-to-right, the brick was tapped down to the appropriate height. The next brick was then buttered and shoved. Once the entire row was laid, it was double-checked to be level and flush. This was repeated for each brick course (layer). Because of the $1/10^{th}$ scale, traditional masonry tools could not be used. Instead, an icing bag with a 22.2mm wide tip per-

mitted rapid application of a fairly uniform mortar layer (across 28.58mm wide brick), which was refined with a small metal spatula. Only six courses were constructed per day to prevent mortar overloading due to self-weight. Sufficient strength gain occurred overnight to permit construction of the next six courses.

Given the mortar's high water content, shrinkage-based cracking was a concern. Traditional solutions employing wet burlap to slow curing proved inappropriate because of interference with carbonation due to the heavy lime content. Acceptable results were achieved using a wax-paper tenting system that was opened daily for approximately six hours during each day of construction and the four days following. Otherwise, the sample was sealed. This generated a slower curing would have occurred under unlimited oxygen. No wall was tested less than 35 days after construction.

The only other wall components were 2.0mm thick oak lintels atop each window to provide support the bricks above (Fig. 20). Wood was selected instead of metal or stone to meet scaling stiffness requirements. The lintels were double-coated with polyurethane to prevent mortar desiccation. The lintels extended into the mortar joint approximately half a brick length beyond the window on each side emulating field practices. Loading details are summarized elsewhere [21, 22].

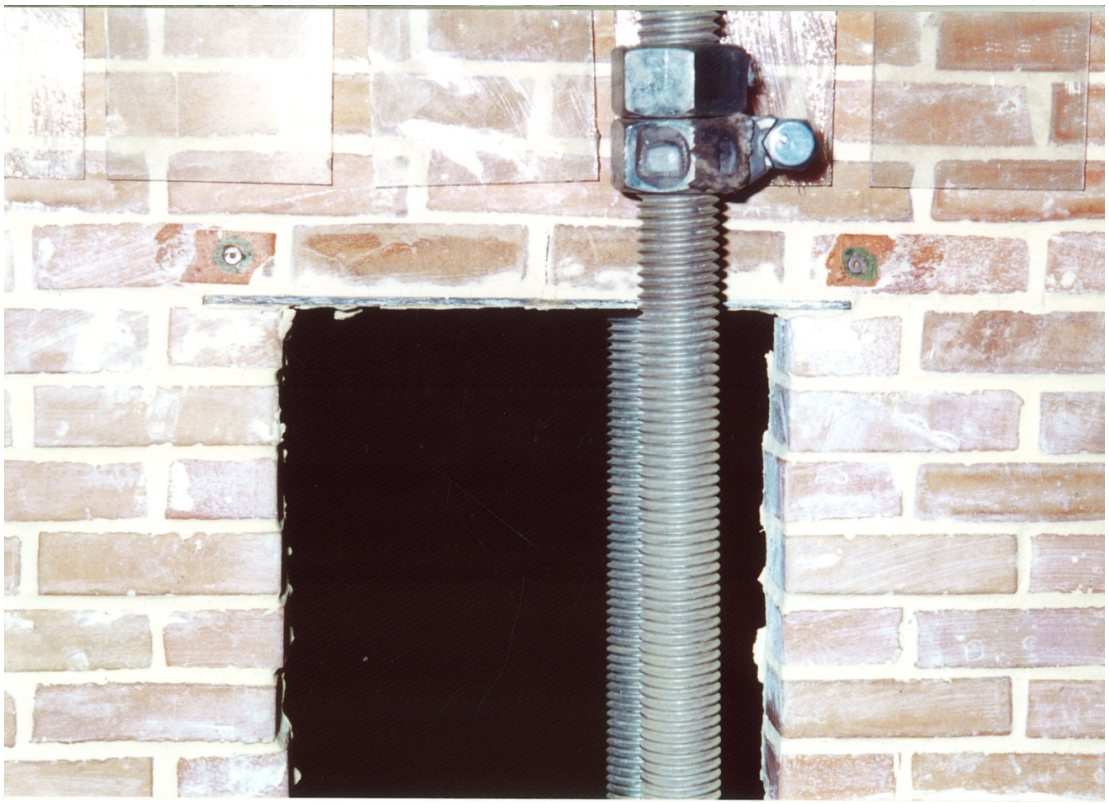

Fig. 20. Window opening with oak lintel visible.

6. Experimental testing

The two tests (Test 4 and Test 5) reported herein for verification were part of a six-test program some of which is reported elsewhere [24]. The scale-model Tests 4 and 5 each included two unreinforced brick walls (named West and East), which were respectively supported by shallow and deep footings. These were subjected to different loads but were otherwise identical. Displacements of buildings, the soil surface, and the excavation wall were recorded at multiple stages of the excavation process.

Once the model buildings were fully installed, the data collection began by establishing an initial zeros point for electronic and manual instrumentations. To measure building model movements, a combination of electronic extensometers and foal gauges were applied to the corners and various other points across the walls to collect both vertical and horizontal displacement, in which accuracy of the dial gauges was ranged from 0.00254mm to 0.0254mm. For each building, vertical and horizontal measurements were at four corners and third-points horizontally and half-points vertically.

Prior to excavation, the building models were examined at close range for pretest damage. During testing, crack identification had to be conducted from a distance with binoculars to avoid interfering with the experiment. Thus, crack measurement had to be postponed until the testing was complete. The emergence of cracks was documented at each stage but could not be measured until the testing was complete. Therefore, crack size was only indicated at the excavation design grade or at the final reading. Additionally, herein it was hard to measure accurately the size of the smallest crack, particularly less than 0.5mm, which reported as 0.1mm.

Dial gauges with the sensitivity of 0.0254mm were distributed across the surface of the testing chamber while electronic extensometers (transtek DCDTs) with the accuracy of 0.0254mm were buried to measure wall and soil mass displacements. Additionally, five levels of mechanical extensometers were placed on the front side of the excavation wall for measurement of horizontal displacements and dial gauges attached on the top of the excavation wall to measure both vertical and horizontal movements.

Excavation occurred in 12 stages of equal depths with an additional three stages for the post-tensioning of the anchors at each level. Details herein are reported for the excavation at design grade. These corresponded to excavation depths of 1.22 in Test 4, and 1.09m in Test 5 (see [24] for a detailed description of the excavation process). At the end of testing, the cumulative displacements and cracking occurring throughout the excavation process were recorded for benchmarking.

7. Experimental results and discussion

To validate the experiments, the results were scaled and plotted atop published field measurements [43, 44, 45]. Validations were made from lateral excavation wall movements, free field surface soil settlement, vertical building movement, and building damage patterns.

Lateral excavation wall movements observed by Boone [43] for an excavation 20m in depth and over 650m long through glacial till and a highly, over-consolidated glaciolacustrine sand, silt, and clay deposit are shown in fig. 21. The excavation was generally supported by wide-flange steel beams combined to vertical spacing of struts ranged from 2.4m to 5.8m. In general, the experimental data when scaled to a factor of 10 was not dissimilar. Boone's final displacements ranged from 0.12% to 0.18% of the excavation depth, while the experimental results were around 0.07-0.08% of the excavation depth. The smaller displacements from the experiments can be understood as an artefact of the more shallow excavation depth of the laboratory tests.

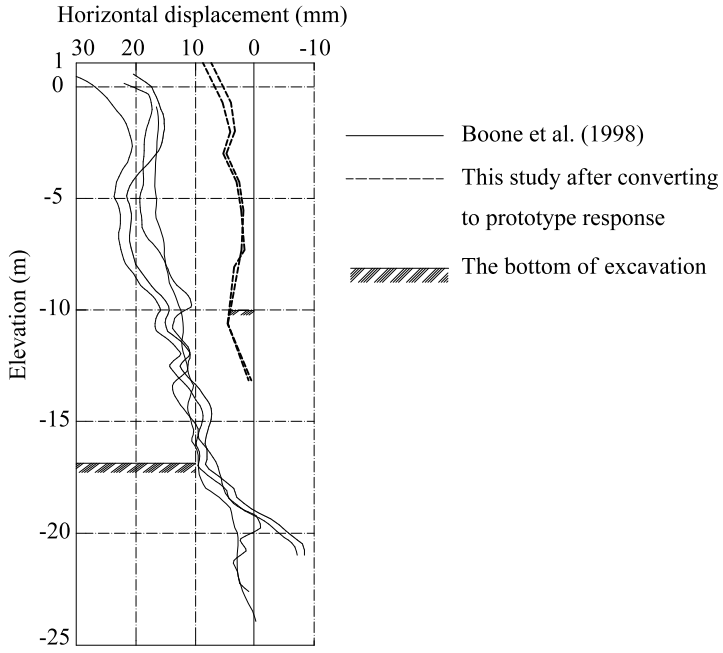

Figure 21. Horizontal displacements of the excavation wall

The second area of comparison is free field surface settlements. These also showed reasonable results when plotted atop field data collect by Peck [44] as shown in fig. 22. The experimental data were in the middle of region I for surface movement in sand with average workmanship, and the maximum vertical displacement of FF was around 0.7%H, where H is the depth excavation. Additionally, the trough profile shape was similar to those proposed by Peck [44].

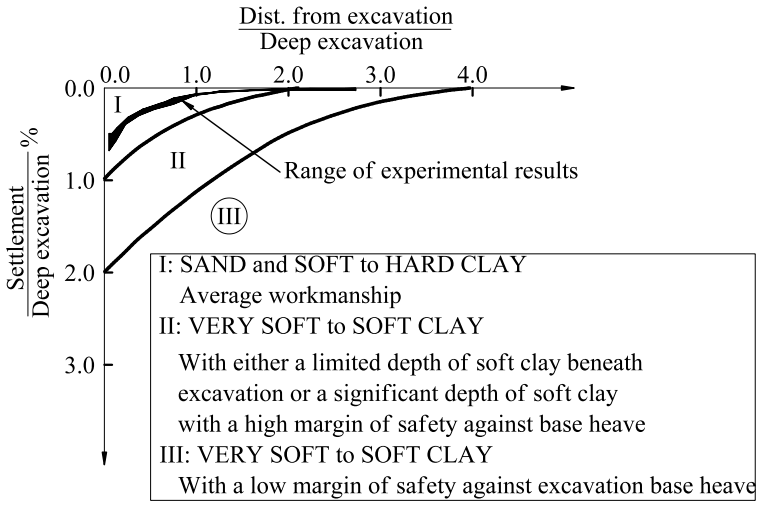

Figure 22. Ground movements in free field region overlain on field results reported by Peck [44]

The third area of comparison was vertical building movements. Boone [43] published vertical displacements for four load-bearing masonry buildings for the abovementioned excavation. The structures ranged in height from 5.5m to 6.7m and in length from 10.9m to 29.0m (scaled up experimental walls were 6.1m x 18.3m). The trends were similar in response shape, even though the experimental wall movements were generally larger (maximum 60mm when scaled up) versus the field observations (maximum 20mm). The difference can be understood as the extreme proximity of the experimental buildings to the adjacent excavation, (Figure 21).

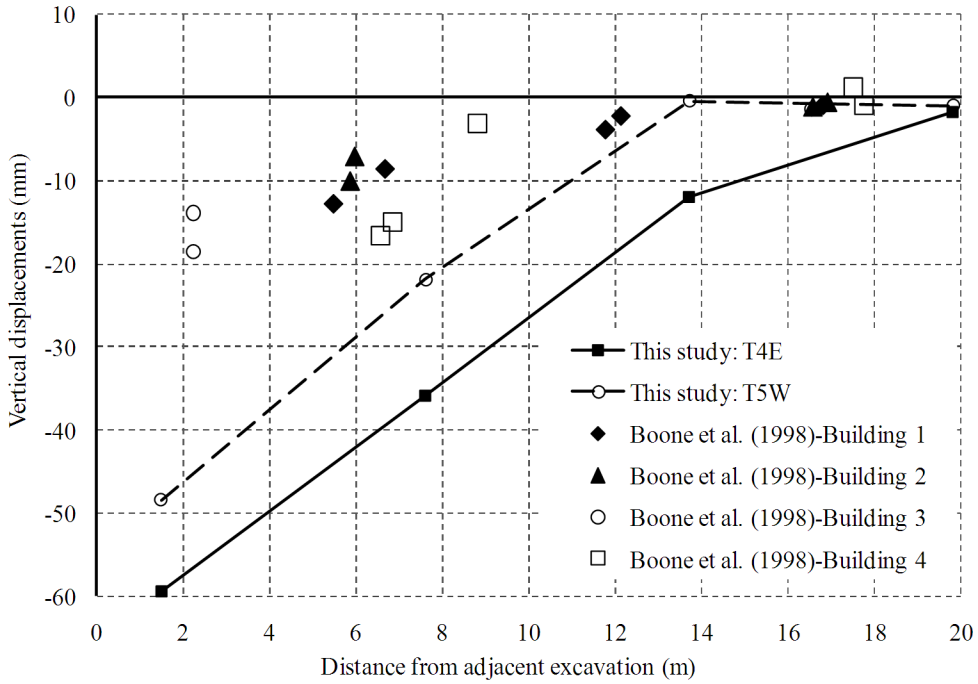

Figure 23. Vertical displacements of the bottom building

The final validation area was damage patterns in the masonry. The general damage and distortion patterns, magnitudes, and cracking densities were commensurate with previously reported cases [43, 44]. The major difference was that damage was more distributed over the entirety of the model, as there were no roof or floor elements to act as diaphragms. Cracks on the scale model propagated from the building bottom toward the building top, in which most of crack appeared on brick-mortar interface that was parallel to diagonal lines of the windows. In the half of the building model closest to the excavation face, the diagonal crack parallel to diagonal lines of the window from a bottom left corner to a top right corner and in another building model, cracks appeared in opposite direction (Figure 24a and b). This observation was consistent to the cracks on real building (Figure 24c). Model damage across the top was due to the lack of a confining roof member. The model walls generally showed diagonal shear cracking, similar to that recorded by the lead author at a site in central Illinois in 2001 (fig. 25), where damage was heavily concentrated in the front lower corner and around the windows.

a) Test 4 at end of study (excavation from right side)

b) Test 5 at end of study (excavation from right side)

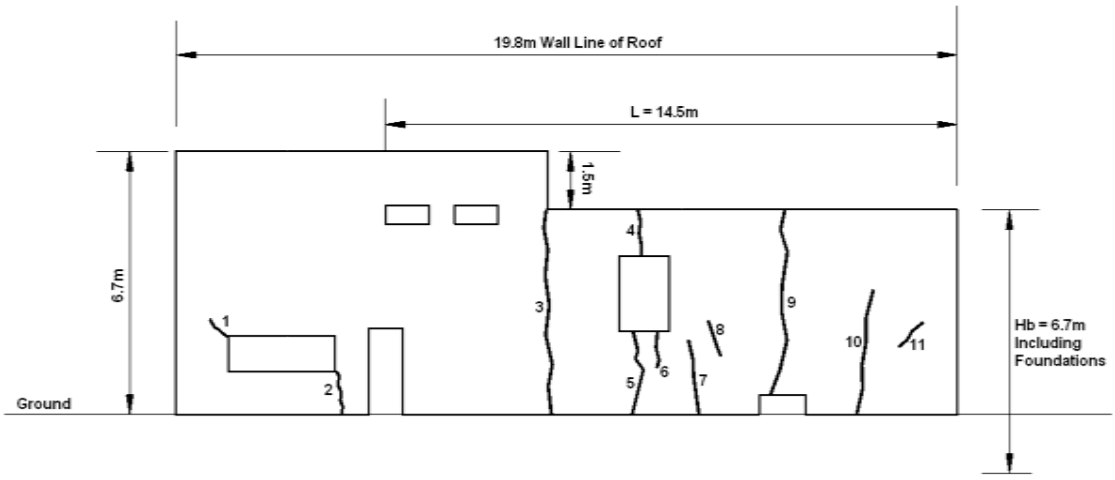

c) Cracks in a real building (adapted from Boone et al. 1998)

Figure 24. Cracks on the building model.

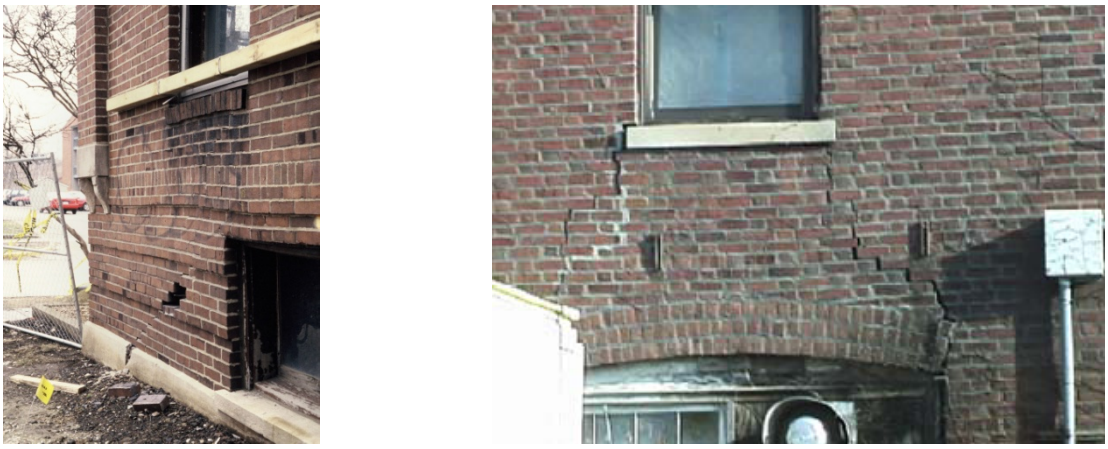

a) Front corner of building b) Ground floor and first floor windows

Fig. 25. Adjacent excavation induced damage at a building in central Illinois 2001

8. Conclusions

By following similitude requirements and using modifications of traditional materials (e.g. shale, lime) and historic building practices (e.g. preweting bricks), relatively small-scale ($1/10^{th}$ scale) masonry products can be manufactured that successfully generate masonry building response for 1g, pseudostatic soil-structure. To develop appropriate materials, first an extensive understanding must be achieved of the materials to be modelled by studying the historic records and recent testing data. As part of the material development programme, appropriate testing protocols must be adopted and/or adapted. The success of the developed materials was verified by comparing lateral wall displacements, surface soil settlement, vertical building response, and cracking patterns. This enables the collection of data that is not usually accessible (e.g. within the soil mass, beneath the building foundations).

References

[1] Wood DM. Geotechnical Modelling. Oxfordshire: Spon Press; 2004.
[2] Shaughnessy EJ, Katz IM and Schaffer JP. Introduction to Fluid Mechanics. Oxford, England: Oxford University Press; 2005.
[3] Langhaar H. Dimensional Analysis and Theory of Models. New York, NY: John Wiley & Sons, Inc.; 1951.
[4] Neto C, Correa M, Ramalho M. Proposal of a Test Specimen to Evaluate the Shear Strength of Vertical Interfaces of Running Bond Masonry Walls. Canadian Journal Civil Engineering 2008; 35(6):567-73.

[5] Dennis S, Baylot J, Woodson S. Response of 1/4-scale Concrete Masonry Unit (CMU) Walls to Blast. Journal Engineering Mechanics 2002; 128(2):134-42.
[6] Laursen P, Ingham J. Structural Testing of Large-scale Posttensioned Concrete Masonry Walls. Journal of Structural Engineering 2004; 130(10):1497-1505.
[7] Tomazevic M, Klemenc I. Seismic Behaviour of Confined Masonry Walls. Earthquake Engineering & Structural Dynamics 1997; 26(10):1059-71.
[8] Altin S, Anil Ö, Kara M, Kaya M. An Experimental Study on Strengthening of Masonry Infilled RC Frames Using Diagonal CFRP Strips. Composites, Part B: Engineering 2008; 39(4):680-93.
[9] Kakaletsis D, Karayannis C. Influence of Masonry Strength and Openings on Infilled R/C Frames under Cycling Loading. Journal Earthquake Engineering, 2008; 12(2):197-221.
[10] Turer A, Korkmaz S, Korkmaz H. Performance Improvement Studies of Masonry Houses Using Elastic Post-tensioning Straps. Earthquake Engineering & Structural Dynamics, 2007; 36(5):683-705.
[11] Manos G, Yasin B, Valiasis T. Small Scale Model Simulation of the Cyclic Behavior of Infill Brick Panels. Proceedings Sixth North American Masonry Conference, June 6-9, 1993, Philadelphia, PA; 1:359-70.
[12] El Gawady MA, Lestuzzi P, Badoux M. Static Cyclic Response of Masonry Walls Retrofitted with Fiber-reinforced Polymers. Journal of Composites for Construction, 2007; 11(1):50-61.
[13] Zarnic R, Gostic S, Crewe A, Taylor C. Shaking Table Tests of 1:4 Reduced-scale Models of Masonry Infilled Reinforced Concrete Frame Buildings. Earthquake Engineering & Structural Dynamics, 2001; 30(6):819-34.
[14] Tomazevic M, Klemenc I. Verification of Seismic Resistance of Confined Masonry Buildings. Earthquake Engineering & Structural Dynamics, 1997; 26(10):1073-88.
[15] Henderson R, Fricke K, Jones W, Beavers J, Bennett R. Summary of a Large- and Small-scale Unreinforced Masonry Infill Test Program. Journal Structural Engineering, 2003; 129(12):1667-75.
[16] Murthy C, Hendry A. Preliminary Investigation of the Shear Strength of One-sixth-scale Model Brickwork. Technical Note, No. 65, 1965, London: British Ceramic Research Association.
[17] Harris H, Labrouki B, Lafis S. Material Characterization for Direct Modelling of Reinforced Block Masonry Structures. Proceedings Fifth North American Masonry Conference, June 3-6, 1990, Illinois; 2:639-50.
[18] Abrams D. Response of Unreinforced Masonry Buildings. Journal Earthquake Engineering, 1997; 1(1):257-73.
[19] Buckingham E. On Physically Systems: Illustrations of the Use of Dimensional Equations. Physics Reviews 4, 1914; 345-76.
[20] Rayleigh Lord, (Strutt JW). The Principle of Similitude. Nature 95, 1915; 66-8.

[21] Laefer DF, Long JH, Cording EJ, Erkal A, Truong Hong L. Strength-scaled Unreinforced Masonry Building Materials for Scaled Soil-structure Experimentation – Theoretical Considerations. Journal of Testing and Evaluation, ASTM, 2010; 38(4). DOI: 10.1520/JTE102420.
[22] Laefer DF. Prediction and Assessment of Ground Movement and Building Damage Induced by Adjacent Excavation. Ph.D. Thesis, University of Illinois at Urbana-Champaign, Urbana, III, 2001.
[23] Peck, R. B., Hanson,W. E., and Thornburn, T. H., *Foundation Engineering*, 2nd ed., John Wiley: New York 1974.
[24] Laefer D, Ceribasi S, Long J, Cording E. "Predicting Reinforced Concrete Frame Response to Excavation Induced Settlement." J. Geotechnical & Geoenvironmental Eng., ASCE, 2009, http://dx.doi.org/10.1061/(ASCE)GT.1943-5606.0000128.
[25] Mitchell C, Mitchell G. Brickwork and Masonry, A Practical Text Book for Students, and Those Engaged in the Design and Execution of Structures in Brick and Stone. London: B.T. Batsford Ltd.; 1904.
[26] Braley EL. Brickwork: A Comprehensive Treatise on the Theory and Practice of the Handicraft of the Bricklayer, Including an Exposition of the Manufacture of the Customary Materials, with Some Notes on the Measurement of Brickwork. London: Sir Isaac Pitman and Sons Ltd.; 1947.
[27] Garrett AJW. Brickwork Including Its Bond, Manufacture and Material used in Connection Therewith. London: Crosby Lockwood and Son Ltd.; 1948.
[28] Laefer DF. Performance Expectations of Early 20th Century Urban American Building Foundations. GeoCongress 2008: Geosustainability and Geohazard Mitigation, GSP No.178, 2008, ASCE, New Orleans, LA; 960-7.
[29] Laefer DF, Boggs J, Cooper N. (2004). Engineering Properties of Historic Brick – Variability Considerations as a Function of Kiln Type. J. Am. Inst. Cons. Historic & Artistic Works, AIC Fall/Winter; 43(3):255-72.
[30] ASTM Standard C109/C109M: Standard Test Method for Compressive Strength of Hydraulic Cement Mortars. Annual Book of ASTM Standards, ASTM International, West Conshohocken, PA, 1999.
[31] ASTM Standard C270-89: Standard Specification for Mortar for Unit Masonry. Annual Book of ASTM Standards, ASTM International, West Conshohocken, PA, 1989.
[32] Pluijm R, Vermeltfoot A. Bond Wrench Testing. Proceedings of the Fourth International Masonry Conference, Proceedings of the British Masonry Society Masonry, 1995; Ed. West HWH; 7(1):225-31.
[33] Ribar JW, Dubovoy VS. Investigation of Masonry Bond and Surface Profile of Brick. Masonry Materials: Design, Construction and Maintenance, ASTM Special Technical Publication 992, ASTM, PA, 1988; Ed. Harris HA; 33-7.
[34] ASTM Standard, C67-94: Standard Test Methods for Sampling and Testing Brick and Structural Clay Tile. Annual Book of ASTM Standards, ASTM International, West Conshohocken, PA, 1994.

[35] Rao RNS. Experimental Investigation on Structural Performance of Brick Masonry Prisms. Proceedings of the International Conference on Masonry Structural Systems, Austin, Texas, Designing Engineering and Constructing with Masonry Products, Ed. Johnson FB; Houston, Texas: Gulf Publishing Co.; 1969, p. 74-9.
[36] Pieper K, Trautsch W. Shear Tests on Walls. Proceedings of the Second International British Masonry Conference; Ed. West HWH, Speed KH. British Ceramic Research Association, London, April 12-15, 1970: 140-3.
[37] Ritchie T, Davison JI. Factors Affecting Bond Strength and Resistance to Moisture Penetration of Brick Masonry. Symposium on Masonry: Presented at the 65th Annual Meeting of the American Society for Testing and Materials, New York, June 28, 1962, ASTM Special Technical Publication 320, ASTM, Philadelphia: 16-30.
[38] Beall C. Masonry Design and Detailing for Architects, Engineers, and Contractors. 3rd Ed. New York: McGraw-Hill, Inc.; 1993.
[39] Mulligan JA. Handbook of Brick Masonry Construction. New York: McGraw-Hill Book Company, Inc.; 1942.
[40] Lenczner D. Strength and Elastic Properties of the 9-in. Brickwork Cube. Transactions of the British Ceramic Society, 1966; 65(6):363-82.
[41] ASTM Standard, E518-80: Standard Test Methods for Flexural Bond Strength of Masonry. Annual Book of ASTM Standards, ASTM International, West Conshohocken, PA, 1980.
[42] Mueller CG. Behaviour of Model-Scale Tieback Walls in Sand. PhD Thesis, University of Illinois, 2000.
[43] Boone SJ. Ground-Movement-Related Building Damage. J. Geotechnical & Geoenvironmental Eng., ASCE, 2002; 122(11): 886-95.
[44] Peck RB. Deep excavations and tunneling in soft ground. Proceedings of the 7th International Conferences on Soil Mechanics and Foundation Engineering, State of the Art Volume, Mexico City, Mexico, 1969, pp. 225-290.
[45] Boscardin M, Cording E. Building Response to Excavation-Induced Settlement. J. Geotech. Eng., 1989; 115(1): 1-21.

Table Captions

Table 1 Properties of models used in experimental 1g masonry studies.

Table 2 Expected prototype performance and resultant experimental values.

Table 3 Mortar mix by weight and parts.

Table 4 Munsell colour chart description of bricks.

Figure Captions

Fig. 1. a) Section b) Plan of experimental set up.

Fig. 2. Schematic details shown of masonry wall

Fig. 3. Formwork shown for laying discrete URM footings.

Fig. 4. Oversanding in lime mixes.

Fig. 5. Mortar strength as a function of bentonite and air entrainment levels.

Fig. 6. Mortar cubes resulting from casting in 5.1cm x 5.1cm brass molds.

Fig. 7. Oversized cast mortar samples from which 5.1cm x 5.1cm samples were cut.

Fig. 8. Quarter-scale bricks shown in comparison to prototype brick in stationary, electric kiln.

Fig. 9. Brick compressive strength by colour designation

Fig. 10. Kiln yield by colour designation.

Fig. 11. Comparative compressive strength by end condition.

Fig. 12. Photograph of tensile brick testing.

Fig. 13. Shear testing results on triplets with no confining stress at 21 and 28 days

Fig. 14. Tensile testing via a no-moment connection.

Fig. 15. Close up of damaged URM wall at end of testing; cracks coloured post-test with marker after being measured.

Fig. 16. Examples of Young's modulus of five-course high brick prisms.

Fig. 17. Photograph of bricks being laid.

Fig. 18. Two model walls shown in their transport frames.

Fig. 19. Wall in place awaiting testing.

Fig. 20. Window opening with lintel visible.

Fig. 21. Horizontal displacements of the excavation wall.